ROYAL SOCIETY
OF CHEMISTRY

COMMUNICATION

Check for updates

Dynamic bonds transform ion transport mechanisms in polymeric covalent adaptable networks

Mohammad Rezayani,[a] Farhad Sharif ⓘ *[a] and Hesam Makki ⓘ *[b]

This study unravels the mechanisms by which dynamic covalent bonds facilitate ion transport in poly(ethylene oxide)-based covalent adaptable networks (CANs), designed for solid polymer electrolytes. Our findings reveal how CANs differ fundamentally from traditional static PEO networks in their ion conductivity behavior. Through molecular dynamics simulations, we show that dynamic bonding creates temporary "corridors" for lithium-ion movement *via* reversible bond breaking and reformation, without altering the network topology. Unlike static networks, which rely on structural loosening for ion diffusion, dynamic bonding uniquely enhances ion transport by inducing local bond rearrangements that create transient structural fluctuations, increasing ion mobility up to 2.8-fold in dense networks. Importantly, these transient structural changes do not alter the overall pore distribution in the network. Instead, the dynamic reactions transform blocked pathways — previously dead-ends — into reversible gates that open and close, effectively regulating ion transport. This mechanism provides a pathway to improve ion conductivity while preserving mechanical integrity.

New concepts

This study introduces a novel ion transport mechanism in poly(ethylene oxide)-based covalent adaptable networks (CANs), where dynamic bond exchange actively facilitates ion mobility. Unlike conventional polymer networks, which rely on structural flexibility for ion transport, we demonstrate that dynamic bonding creates transient, reversible "gates" that prevent ion trapping and enhance interchain hopping, enabling efficient ion diffusion without altering the network's overall pore structure. This challenges the traditional view that increasing crosslink density restricts ion transport. Instead, we show that dynamic bonds mitigate these constraints by transforming blocked pathways into active transport channels. While previous studies have observed ion conductivity enhancements in CANs, the underlying mechanism has remained unclear. Our work isolates the direct role of dynamic bonding, revealing that ion conductivity can be tuned independently of geometric constraints. By uncovering how dynamic covalent reactions regulate ion transport at the molecular level, this study provides a new design paradigm for ion-conductive materials. This insight enables the development of solid polymer electrolytes with enhanced conductivity and preserved mechanical integrity, paving the way for next-generation energy storage devices.

1. Introduction

Polyethylene oxide (PEO)-based covalent adaptable networks (CANs) have emerged as a promising class of materials for energy storage devices, owing to their flexibility, non-crystallinity, and the strong Li-ion solvation ability of PEO.[1–8] Compared to traditional static polymer networks, CANs exhibit significantly enhanced ion transport properties, which is attributed to dynamic exchange reactions[9] often provided by the incorporation of disulfide bonds within the network structure.[10,11] While extensive experimental studies have reported ion transport enhancement in PEO-based CANs compared to conventional PEO-based membranes,[3,12–18] the specific mechanistic role of dynamic

bonds in this enhancement remains not fully understood. These mechanisms are essential for improving the efficiency of CAN-based membranes through the molecular design of the network.

The performance of PEO-based membranes is predominantly defined by Li-ion transport, which takes place through three primary mechanisms described by a Rouse-based model:[19,20] (i) intrachain Li-ion movement along the polymer backbone, (ii) cooperative motion of Li-ions with PEO segments, and (iii) Li-ion hopping between polymer chains.[1,19–21] While these mechanisms are well established and valid for PEO-based CANs, the role of dynamic bonds in modulating them remains unclear. Specifically, it is not yet fully understood whether dynamic bonds enhance Li-ion mobility by altering segmental dynamics and network rearrangement or if it primarily affects interchain hopping pathways.

Molecular dynamics (MD) simulation is a powerful tool for investigating polymeric membrane dynamics at the molecular

[a] *Department of Polymer and Color Engineering, Amirkabir University of Technology, 424 Hafez Ave., Tehran, Iran. E-mail: sharif@aut.ac.ir*

[b] *Department of Chemistry and Materials Innovation Factory, University of Liverpool, Liverpool L69 7ZD, UK. E-mail: H.Makki@liverpool.ac.uk*

scale, which is often challenging to probe directly through experiments. MD methods have been extensively applied to study the diffusion mechanisms of ions in PEOs without dynamic bonds.[22–24] However, modeling dynamic bonding presents a complex challenge that requires accounting for various concurrent phenomena. These include cross-linking reactions, reversible exchange reactions between reactive groups, and the diffusion of ionic groups and polymer dynamics. Coarse-grained (CG) MD simulation offers a simplified reactive scheme and captures the time scales associated with these reactions. However, CG models often provide only qualitative insights into diffusion due to the use of softer interaction potentials and limited chemical specificity.[25,26] Consequently, validating CG results with atomistic simulations and experimental studies is essential to ensure accuracy and reliability.

This study investigates the diffusion behavior of Li-ions in polymeric CANs. We simulated a series of PEO-based systems with dynamic disulfide bonds and varying crosslinking densities.[3] The primary objective is to isolate the intrinsic effects of dynamic exchange reactions on network structure and ion transport. To achieve this, we employed PolySmart,[27] a versatile reactive MD simulation tool, to construct PEO networks at the CG scale. We then implemented an additional reaction scheme to model dynamic exchange reactions between disulfide linkages and computed the structural and dynamic properties of the membranes with and without these reactions. Moreover, we studied the effect of exchange reaction kinetics on ion diffusion behavior. Finally, a reverse mapping scheme was applied to translate CG models into atomistic representations, enabling the validation of key structural and diffusional properties. Furthermore, the model predictions were compared with existing experimental data for additional validation.

2. Method

All the simulations were performed using GROMACS (Version 2022-2),[28] utilizing the leap-frog integration algorithm.[29] The thermodynamic parameters of temperature and pressure were controlled by a V-rescale thermostat[30] at 295 K and Parrinello–Rahman barostat[31] at 1 bar for both atomistic and CG simulations. For atomistic simulations, to treat the long-range coulombic interactions, we employed particle mesh Ewald (PME) summation[32] with the cutoff distance set at 1 nm. Also, the van der Waals (VdW) pair interactions were described by the 12–6 Lennard-Jones potential with the cut-off distance of 1 nm. Periodic boundary conditions were employed in three directions (xyz), and VMD[33] was used to visualize the simulation trajectories. The detailed procedure of parametrization and simulation of the system in both atomistic and CG scales is provided in the SI (Sections S1 and S2).

Polymerization and dynamic exchange reactions were modeled using PolySMart,[27] a Python package built on a reactive MD framework based on the Martini 3 force field. This package is specifically designed for polymerization and crosslinking reactions, allowing the construction of polymer models with specified reaction conversion and without any limitation on architecture

or chemistry. This methodology consists of several loops of reactions, each including a static reaction step, which is followed by an MD simulation step. Thus, at each reactive static step, PolySMart identifies the reactive species (beads) in the simulation box that are located within a specified and given-as-input cutoff distance. Then, based on the probability of the occurrence of each reaction, given as input – a number between 0 and 1, the software randomly selects among those beads and forms or breaks the bonds between them by updating the relevant topology information in the force field files. Each reaction cycle is then followed by an MD simulation step for a user-defined duration (e.g., 1 ns), and this reaction/MD loop continues until a specified termination condition (e.g., a defined number of cycles or target conversion) is reached.

The input configurations to PolySMart were made by inserting an appropriate number of EO, PET, and LiTFSI randomly in a sufficiently large simulation box (20 × 20 × 20 nm). After energy minimization and initial compression of the box, the cross-linking simulation was performed during MD simulation with a time step of dt = 10 fs, and the termination condition of EO conversion = 99%. The details of the polymerization procedure can be found in Section S3 of the SI. It should be noted that all the simulations have been performed with at least two independent initial configurations, and the average of the parameters is reported.

After achieving the desired degree of crosslinking, the network was further equilibrated with a 100 ns NPT simulation. Next, the bond exchange process was introduced using a user-defined exchange probability ($P_{exchange}$). In this approach, two disulfide groups within a cut-off distance of 0.412 nm (twice the S–S bond length) are eligible to exchange bonds. A list of all possible bond pairs is generated, and, in each cycle, a subset is randomly selected for exchange based on the specified $P_{exchange}$. For example, for a $P_{exchange}$ = 0.5, half of the eligible bond pairs are exchanged, while with $P_{exchange}$ = 1, all pairs on the list undergo exchange reaction. Thus, the frequency of dynamic bond exchange can be controlled through the $P_{exchange}$ defined in the input file. This approach mimics the effect of temperature on reaction rates in real polymer systems, where elevated temperatures facilitate bond exchange by increasing molecular mobility and exchange probability, making this control experiment more relevant for understanding thermally driven dynamic behavior.[3] Finally, the trajectories from the dynamic exchange simulations were analyzed to extract key transport and structural properties.

Radial distribution function (RDF), a statistical measure used to describe the variation of particle (i) density as a function of distance from a reference particle (j), which is shown as $g_{i-j}(r)$, and indicates the likelihood of finding neighbors at different distances,[34] was calculated for various chemical groups. The coordination number (CN), which is defined as the number of atoms, ions, or molecules that are in a specified spatial range (typically defined by a cutoff radius) from a central atom or ion, is also used to provide a measure of how many nearest neighbors surround a given particle in a system.[35]

To quantify the structural parameters of the polymer network, PoreBlazer (v4.0)[36] is utilized, which has been employed successfully in similar polymer networks in our recent studies.[34,37,38] This tool, renowned for its ability to analyze pore distribution and microstructural characteristics of polymeric materials, yields valuable insights into their structural properties. Pore limiting diameter (PLD), maximum pore diameter (MPD), and pore size distribution (PSD) are the most important parameters that were calculated and examined using this tool.

The rate of ion diffusion into the polymer matrix is characterized by the self-diffusion coefficient (D_s):

$$D_s = \frac{\sum_{i=1}^{N} D_i}{N} \quad (1)$$

where N is the number of ions, and D_s is the self-diffusion coefficient of a single ion in the polymer network calculated by using the following Einstein relation:

$$D_s = \lim_{t \to \infty} \left(\frac{\langle (r_{com}^i(t) - r_{com}^i(0)) \rangle}{6t} \right) \quad (2)$$

where, $\langle (r_{com}^i(t) - r_{com}^i(0)) \rangle$ is the mean squared displacement (MSD) of diffusing species i, and t is time.

The diffusion coefficient is calculated from the linear part of MSD *versus* time during the simulation in a diffusive regime where particles have made several hops between sites. Moreover, to provide insight into the interaction strength and dynamics between the ion and different parts of the system, we calculated residence time, which is described in Section S4 of the SI.

The Nernst–Einstein equation depicts the relation between ionic conductivity σ of an electrolyte and self-diffusion coefficient D_s of ionic species, as shown below.[39]

$$\sigma = \frac{e^2}{V k_B T} (N_+ z_+^2 D_{s+} + N_- z_-^2 D_{s-}) \quad (3)$$

where e is the elementary charge, k_B the Boltzmann constant, T the temperature in Kelvin, V the volume of the simulation box, and D, z, N, respectively, the self-diffusion coefficient, charge, and number of cations (indicated by a positive sign) and anions (indicated by a negative sign).

For reverse mapping from coarse-grained (CG) to atomistic resolution, a two-step procedure was employed. First, the CG structure was converted to an atomistic representation using the backward technique.[40] Next, the atomistic structure, parameterized with the original OPLS-AA force field, was energy-minimized to resolve any steric clashes introduced during reverse mapping. To ensure proper equilibration, thermal annealing simulations were performed from 800 K to 425 K at a cooling rate of 5 K ns^{-1} under 1 bar pressure, using a 2-fs time step and simulation settings consistent with the CG simulations. Finally, a 100 ns MD simulation at 425 K was conducted to compute the structural and dynamic properties of the atomistic models.

3. Results and discussion

The chemical structures of the monomer, crosslinker, and ionic liquid are shown in Fig. 1a–c. In total, four CAN systems are modeled, with their compositions summarized in Table 1. To control the cross-linking density, the ratios of PET to EO monomer were set at 1 : 25, 1 : 50, 1 : 75, and 1 : 100, corresponding to the systems PET-EO$_{25}$, PET-EO$_{50}$, PET-EO$_{75}$, and PET-EO$_{100}$, respectively. The criteria for the selection of these samples was to ensure a range of compositions with varying application-relevant network densities and ion conductivity for Li-polymer battery applications.[3] The salt concentration (r), defined as the molar ratio of Li to ether oxygens in the network (Li : O), is maintained at an optimal value of $r = 0.1$, as determined experimentally, where, after this concentration, a reverse, decreasing, conductivity behavior is observed.[3] This concentration is consistent across all systems (see Table 1).

3.1. Structural characterization

In ether-based polymers used for solid polymer electrolytes, the concentration of Li-ions is often tuned based on the availability of ether oxygen, which serves as the coordination site for Li-ions. This relationship is critical for optimizing ionic transport properties and improving the efficiency of lithium-ion batteries.[1,41,42]

To investigate the local structure, we analyze the radial distribution function (RDF) of Li and CM beads of EO monomers (see Fig. 1). Consistent with previous studies,[23] we assume that a Li atom is coordinated with oxygen if it falls within the first Li–CM coordination shell. Fig. 2a shows g_{Li-CM} at various cross-linking densities. All RDF plots exhibit a distinct first
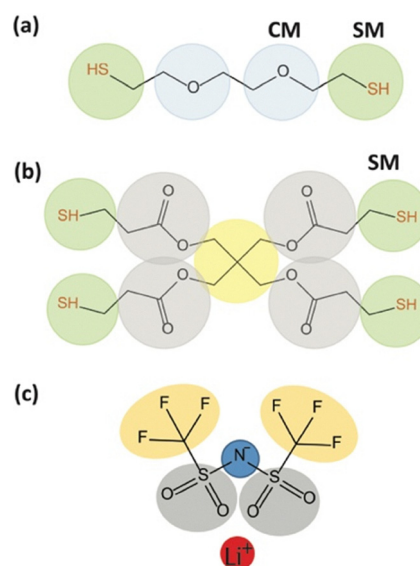

Fig. 1 Chemical structure and mapping scheme of (a) 2,2′-(ethylenedioxy)diethanethiol or (EO), (b) tetrathiol cross-linker, pentaerythritol tetrakis(3-mercaptopropionate) or (PET), and (c) lithium bis-trifluoromethanesulfonimide (LiTFSI). CM: beads containing ether oxygen, and SM: reactive beads. A full description of bead names can be found in (SI, Section S2).

Table 1 Composition of the systems in the simulation box

Sample	PET	EO	Li	TFSI
EO_{25}	50	1250	270	270
EO_{50}	50	2500	520	520
EO_{75}	50	3750	770	770
EO_{100}	50	5000	1020	1020

peak at 0.40 nm and a second, shallower peak at 0.62 nm. The coordination number (CN) plot (right axis in Fig. 2a) further reveals that, on average, at least four oxygen atoms coordinate each Li-ion within a 0.50 nm radius.

Notably, the height of the first RDF peak decreases while the CN values increase as the cross-linking density decreases. In highly cross-linked systems, polymer chains are more constrained, keeping the oxygen atoms of PEO in fixed positions around Li-ions. This leads to a pronounced first RDF peak, indicating a strongly localized coordination shell. Conversely, lower cross-linking densities provide greater flexibility to the polymer network (see MSD analysis of CM beads in Fig. S4 in SI), allowing increased oxygen mobility. This flexibility broadens the RDF peak, indicating a larger spatial spread of oxygen atoms around the Li-ions, and increases the CN values, reflecting greater oxygen accessibility for Li-ion coordination.

Moreover, we proceeded with the analysis in the dynamic network (see the graphical scheme of dynamic exchange in Fig. 2b) with different exchange reaction probabilities:

$P_{exchange}$ = 0.0, 0.5, and 1.0. To better interpret the effect of $P_{exchange}$, we introduced a related metric—the exchanged bond fraction, $F_{exchange}$—which quantifies the average fraction of pair bonds exchanged over the entire simulation (e.g., 10 ns), normalized by the total number of exchangeable disulfide bonds in the system. It is worth noting that $F_{exchange}$ and $P_{exchange}$ exhibit a linear relationship (see Fig. 2c). As shown in Fig. 2c, systems with lower crosslinking density exhibit a higher $F_{exchange}$ compared to more densely crosslinked networks. This behavior reflects the increased flexibility and greater accessibility of disulfide bonds in the loosely connected systems.

Fig. 2d shows the $g_{Li-CM}(r)$ for PET-EO_{25} – the sample with the highest network density and, therefore, the greatest mechanical stability among all[3] – at different $F_{exchange}$. As shown, the first RDF peak height decreases slightly in the dynamic network. While both static and dynamic networks exhibit some degree of polymer flexibility, the presence of dynamic disulfide bonds introduces an additional mechanism for structural rearrangement. These bonds undergo reversible cleavage and reformation, allowing for subtle adjustments in chain conformation. As a result, oxygen atoms can explore a slightly broader spatial range around Li-ions, contributing to a moderate increase in coordination number (CN) and a slight broadening of the RDF peak.

To validate the results of the CG models, we analyze $g_{Li-CM}(r)$, $g_{Li-TFSI}(r)$, and the corresponding CN (for static networks) after
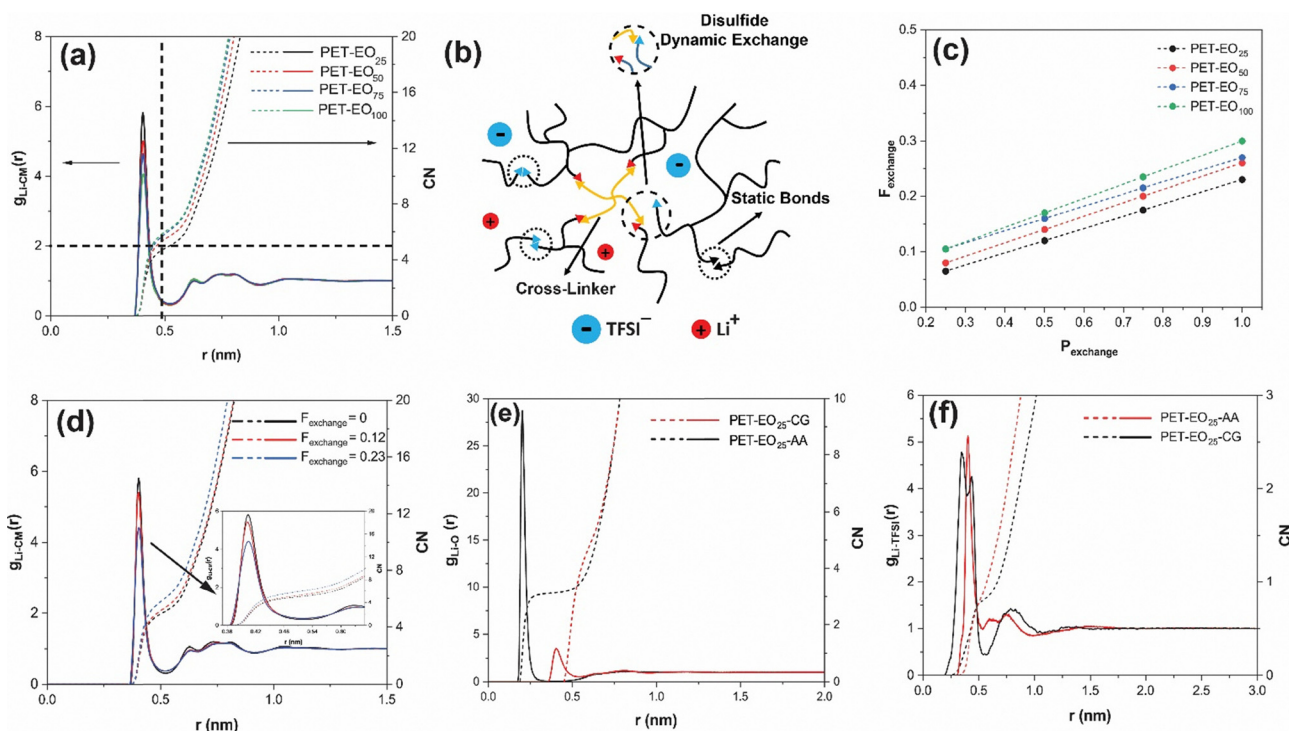

Fig. 2 (a) RDF of Li–CM (ether oxygen) and corresponding CN at different crosslinking densities. (b) Graphical schemes of the dynamic exchange process. (c) Linear relationship between exchanged bond fraction ($F_{exchange}$) and exchange reaction probability ($P_{exchange}$) for all systems, (d) RDF of Li–CM (ether oxygen) and corresponding CN at different $F_{exchange}$, (e) RDF of Li–O (ether oxygen) for PET-EO_{25}, and (f) RDF of Li–TFSI on atomistic and CG scales.

reverse mapping and further equilibrating the structures at the atomistic scale for the PET-EO$_{25}$ model (details in Methods). As shown in Fig. 2e and f, the atomistic simulation results follow the same trend as the CG simulations. However, the magnitude of the distance at which the peak occurs differs due to the inherent differences between atomistic and coarse-grained models. Notably, the first coordination peak in the atomistic simulation appears at about 0.22 nm, closely matching the 0.21 nm peak observed in neutron scattering experiments.[43]

An optimized pore structure enhances ion mobility within the polymer matrix, whereas narrow or poorly distributed pores can trap ions and hinder percolation, reducing overall diffusivity.

Specifically, we investigate the pore-limiting diameter (PLD), maximum pore diameter (MPD) (a schematic is shown in Fig. 3a), and pore size distribution (PSD) to assess the impact of cross-linking and dynamic bonds on ion transport pathways. Increasing the cross-linking density results in a more compact structure with smaller transport channels. Fig. 3b illustrates the variation of PLD and MPD as a function of cross-linking density. As shown, both PLD and MPD increase as the cross-

linking density decreases, shifting from approximately 0.35 nm and 0.68 nm to 0.63 nm and 1.15 nm, respectively. Additionally, the variation in pore size is analyzed as a function of $F_{exchange}$ in dynamic networks. Interestingly, PLD, MPD, and PSD remain unchanged across different $F_{exchange}$ (Fig. 3c and d). As shown in Fig. 3d, all membranes exhibit a single, narrow peak corresponding to the most probable pore size of approximately 4.4 nm in the heterogeneous structure, with no significant differences in size distribution across various $F_{exchange}$. Moreover, we analyzed the variations in PLD, MPD, and PSD for all models at the atomistic scale (dashed lines in Fig. 3b–d). As shown, the trends closely align with the predictions of the CG models. The observed shift in magnitudes after reverse mapping and equilibration is attributed to the greater space explored by the probe, which results from the more realistic van der Waals radii of atoms in atomistic models.

3.2. Diffusion behavior

In this section, we aim to disentangle the effects of network topology and dynamic exchange reactions on the diffusion
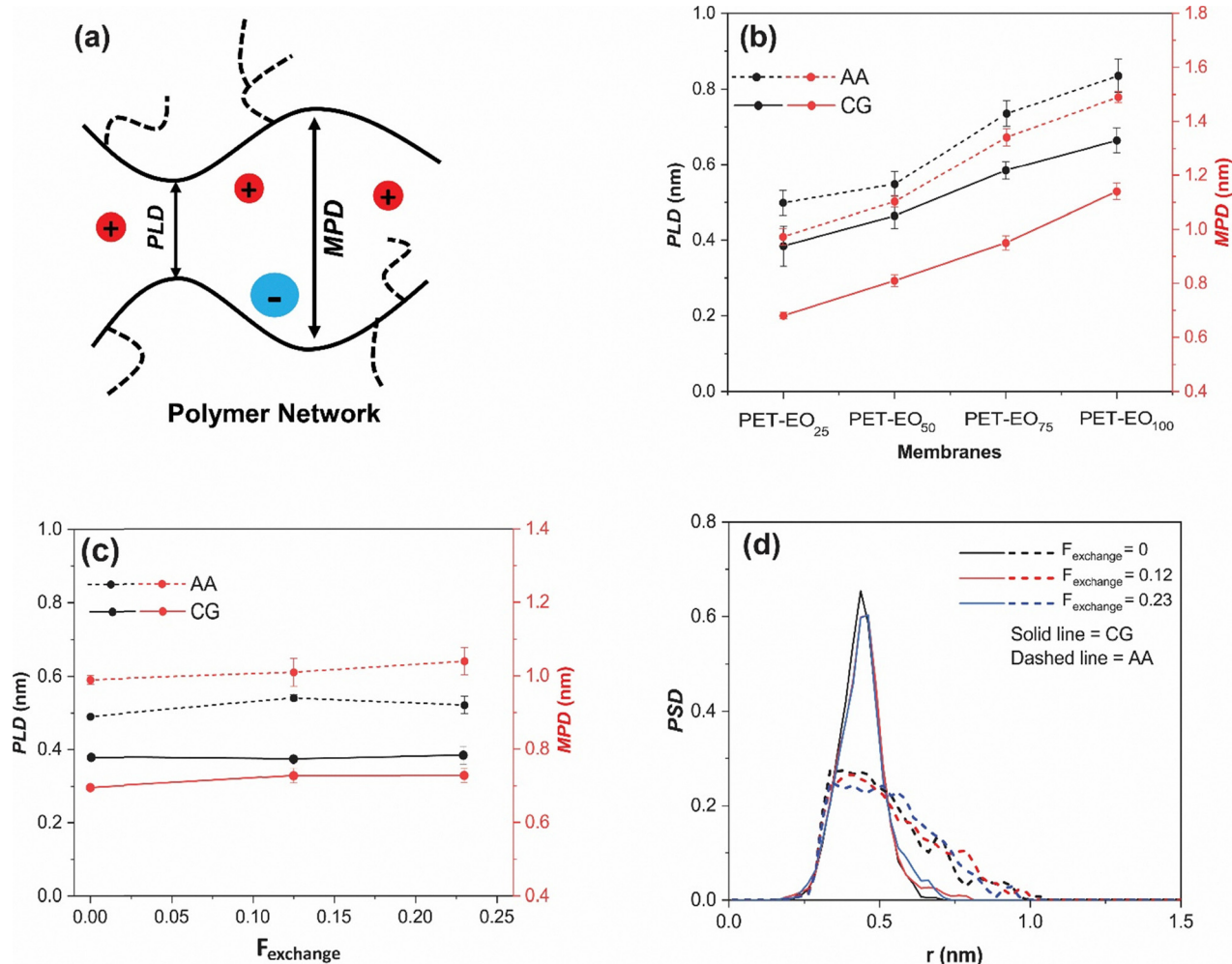

Fig. 3 (a) Graphical schemes of PLD and MPD, (b) pore limiting diameter (PLD) and maximum pore diameter (MPD) of different samples in the static network ($F_{exchange}$ = 0), (c) PLD and MPD variation of PET-EO$_{25}$ as a function of exchanged bond fraction ($F_{exchange}$), and (d) pore size distribution (PSD) of PET-EO$_{25}$ at different $F_{exchange}$. Note that solid lines are on the CG and dashed lines are on the atomistic scale.

behavior of Li-ions. To achieve this, diffusion coefficients were calculated from the mean squared displacement (MSD) of the Li-ions at different $F_{exchange}$ (examples shown in SI, Fig. S5). Fig. 4a displays the diffusion coefficient of Li-ions (D_s) for various networks under different $F_{exchange}$. As shown, D_s increases as the cross-linking density decreases, rising from 0.18 cm^2 s^{-1} in PET-EO$_{25}$ to 0.58 cm^2 s^{-1} in PET-EO$_{100}$.

It is important to highlight that at the CG scale, the smoother interaction potentials between beads often lead to an overestimation of diffusion coefficients compared to atomistic simulations and experimental values under equivalent conditions.[25,26] This discrepancy arises because CG models lack the atomic-level friction and energetic barriers present in atomistic systems, resulting in artificially enhanced ion mobility. However, since the primary goal of this study is to uncover the fundamental mechanisms governing Li-ion diffusion, our focus is on the relative differences in diffusion coefficients across various systems rather than their absolute values. By maintaining a consistent framework, the trends observed in CG simulations remain valid for comparative analysis, even if the exact numerical values deviate from experimental results.

To validate the hypothesis, we calculated the Li-ion MSD and diffusion coefficient for all reverse-mapped models simulated at 425 K, a temperature within the operating range of these polymer electrolytes and above the T_g of models in real conditions.[3,8] The results showed that ion mobility increased as the cross-linking density decreased, a trend consistent with the coarse-grained (CG) results (see Fig. S6 in SI). Additionally, the Li-ions were found to be completely free, with no aggregation observed at either scale (Fig. 2f and SI, Movies M1, M2), which is a crucial characteristic for Li-ion solid polymer electrolytes.[44]

As shown in Fig. 4a, D_s increases significantly with the incorporation of dynamic exchange reactions (increase in $F_{exchange}$). Since ion diffusion is linked to structural relaxation, this enhancement likely arises from the dissociation of disulfide bonds, which affects the structural dynamics of the polymer at higher $F_{exchange}$. More interestingly, dynamic bonding has a more pronounced effect on Li-ion diffusion in denser networks – e.g., in PET-EO$_{25}$, diffusion

increases about 2.5-fold, whereas in PET-EO$_{100}$, the increase is only about 30%.

The diffusion coefficient of TFSI as a function of $F_{exchange}$ is presented in SI, Fig. S7a. Note that due to the stronger affinity of Li-ions compared to TFSI for ether oxygen (see Fig. S7b), the diffusion coefficient of Li-ions is typically lower than TFSI, which is consistent with several reported computational and experimental data.[23,45,46]

To further investigate this effect, the spatial motion of reactive S-containing beads (SM) in PET-EO$_{25}$ is analyzed in both static and dynamic states (Fig. 4b). These results show that in the static state, reactive beads exhibit weaker dynamics, as indicated by the lower MSD slope. However, in the dynamic state, the exchange process increases bead mobility, contributing to enhanced ion transport – an effect consistent with the Li-ion hopping between polymer chains, the third Li-ion transport mechanism described in the introduction.

To study the bond exchange kinetics, we systematically varied the probability of the disulfide exchange reaction ($P_{exchange}$) to control the dynamic disulfide exchange fraction ($F_{exchange}$) and calculated the corresponding Li-ion diffusion coefficients. Fig. 4c shows the Li-ion diffusion coefficient as a function of the $F_{exchange}$. The plot shows that D_s increases exponentially with the $F_{exchange}$. We can argue that by increasing $P_{exchange}$ from 0 to 1, we are decreasing the barrier for dynamic exchange bonds from infinity (no reaction takes place between colliding disulfide groups) to 0 (every colliding disulfide bond undergoes dynamic reaction)—thus increasing $F_{exchange}$ from 0 to about 0.25 (Fig. 4c). This behavior highlights the great potential to regulate ion conductivity by the kinetics of dynamic exchange reactions in solid polymer electrolytes.

We also computed the conductivity of LiTFSI for all samples at different $F_{exchange}$. The conductivity behavior aligns with experimental charge transport measurements,[24] which is expected given the linear relationship between ion diffusion coefficients and charge transport. The experimental conductivity of PET-EO$_{25}$ showed around 1.6-fold increase from static to dynamic state,[3] which is slightly smaller than the 2.8-fold increase predicted by the simulation for the $P_{exchange} = 1$
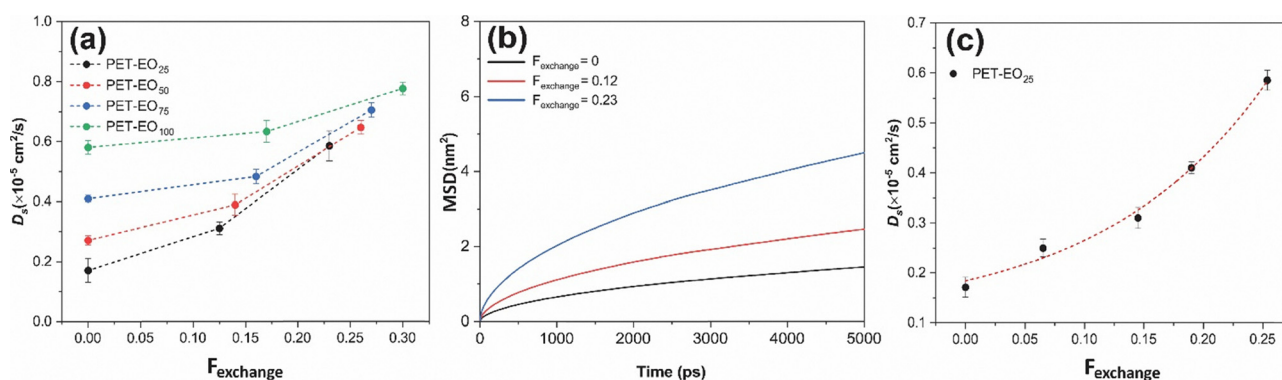

Fig. 4 (a) Diffusion coefficients of Li at different cross-linking densities and exchanged bond fraction ($F_{exchange}$), (b) MSD of reactive S-containing beads for PET-EO$_{25}$ in both the static and dynamic state, and (c) diffusion coefficient of Li-ions as a function of $F_{exchange}$ for PET-EO$_{25}$. The Li concentration for all cases is equal to $r = 0.1$.
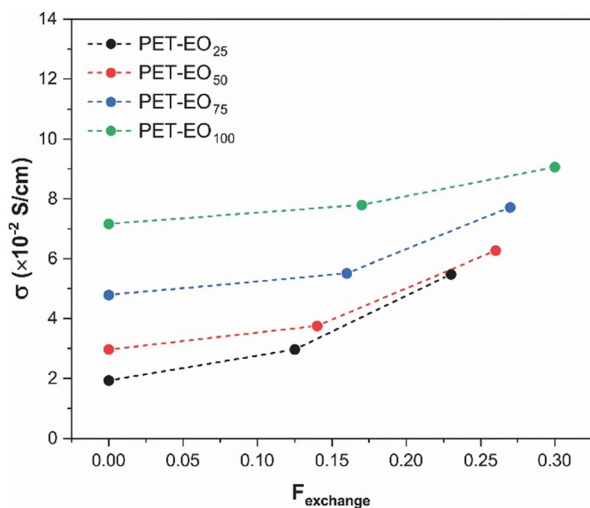
Fig. 5 Conductivity of LiTFSI at different exchanged bond fractions ($F_{exchange}$).

condition (Fig. 5), which is in quantitative agreement with experimental values.[3]

It should be mentioned that in the experimental study by Kato *et al.*,[3] ionic conductivity was measured over a broad temperature range (20–180 °C), all above its glass transition temperature ($T_g \approx -45$ °C), with specific emphasis on 90 °C. These elevated temperatures increase the $P_{exchange}$ by enhancing both segmental mobility and providing the thermal energy needed to overcome the reaction energy barrier.

In our CG simulations, the mobility of chemical groups is inherently comparable to that in experimental systems above T_g, due to the soft interaction potentials and reduced molecular friction.[47] Consequently, the simulated conditions are consistent with the experimental regime. While our classical modeling approach does not explicitly include temperature-dependent reaction kinetics—which would require quantum chemical (*e.g.*, *ab initio*) treatments[48]—tuning the $P_{exchange}$ allows us to effectively explore the relative influence of these kinetic parameters, including those relevant to room temperature behavior.

Beyond thermal control, several alternative strategies exist for tuning the dynamic bond exchange rates at room temperature. These include catalytic approaches (*e.g.*, amines, thiols, phosphines),[49,50] external stimuli (*e.g.*, light, redox, pH changes),[9,51,52] and solvent effects.[53] Such approaches offer promising avenues for enhancing ion transport without requiring elevated temperatures, thus broadening the relevance of our findings to room-temperature battery applications.

Considering both the diffusion coefficient trends and the structural changes in the polymer network, we note that while the pore size distribution remains similar in static and dynamic
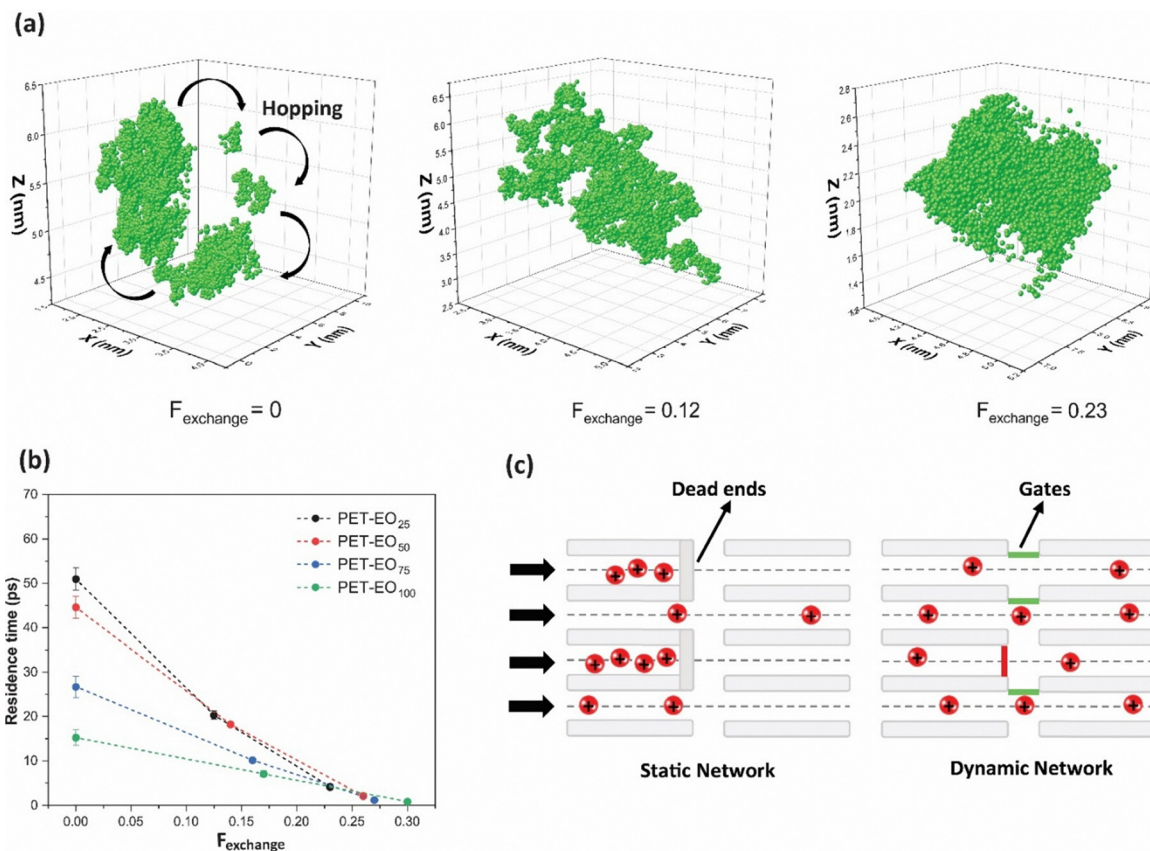

Fig. 6 (a) The trajectory of a single ion (Li) in the static and dynamic network at different exchanged bond fractions ($F_{exchange}$) for PET-EO$_{25}$, (b) residence time of Li near CM beads (ether oxygen of EO), and (c) hypothetical scheme of ion movement in a static and dynamic network (switch–gate mechanism).

states, the increased diffusion in the dynamic network can be attributed to continuous bond exchange. This ongoing rearrangement creates more flexible and adaptable pathways for ion movement, thereby facilitating ion diffusion despite the unchanged pore dimensions and overall network topology within the membranes.

As mentioned, the process of ionic diffusion in PEO-based electrolytes occurs by intrachain or interchain hopping mechanisms.[1,54] The hopping mechanism involves discrete jumps or transitions of particles from one site to another within a polymer matrix. Therefore, we examined the trajectory of a single ion in the PEO network to understand how dynamic bonds affect the diffusion behavior. Fig. 6a shows the trajectory of a single ion in PET-EO$_{25}$, where the single ion undergoes a series of hopping motions, which is directly related to a restricted environment exerted by a tight polymer chain in a static network. As shown, the ion spends a relatively long time at one point and jumps to another point at the right time with the movement of the polymer chain. As the dynamic bonds are applied at $F_{exchange} = 0.12$ and $F_{exchange} = 0.23$, the trajectory is more uniform, and ions move more freely throughout the polymer network.

To better understand the hopping mechanism, we investigated the effects of cross-linking density and dynamic bonding on the residence time of Li-ions near ether oxygen groups in the EO chain (Fig. 6b). Residence time represents the average duration that a Li-ion remains coordinated to either EO groups or anions before transitioning to another chain or coordination site. The results indicate that the residence time of Li near ether oxygen groups decreases from 51 ps in PET-EO$_{25}$ to 15.6 ps in PET-EO$_{100}$ as the cross-linking density decreases. This reduction is attributed to a combination of reduced confinement and enhanced mobility of both Li-ions and PEO chains. More interestingly, the introduction of dynamic bonds significantly reduces the residence time, reaching its lowest value at $F_{exchange} = 0.23$ (e.g., from 51 ps to 5 ps). This suggests that dynamic bonding facilitates a more efficient hopping process by creating open corridors that enhance ion transport.

Overall, the observed structural and diffusion behavior suggests that while free volume and segmental motion play a more pronounced role in ion transport with static changes in the network, e.g., crosslinking density, structure reconstruction becomes the primary factor in improving diffusion by applying dynamic bonds. Therefore, a novel mechanism governing ion transport in the dynamic network is suggested. Specifically, transient structural fluctuations induced by exchange reactions—beyond those arising from thermal motion—significantly enhance ion transport. This behavior can be understood through a "switch-gate" mechanism (Fig. 6c), where dynamic bond exchange, combined with thermal fluctuations, prevents the formation of channel dead ends, thereby facilitating ion movement.

networks, where decreased cross-linking density enhances the ion diffusion due to improved chain dynamics at the expense of deteriorating mechanical properties. In CANs, however, the behavior differs significantly. Our simulations suggest that ion diffusion can increase substantially at very high crosslinking densities, as reversible disulfide bonds facilitate the movement of previously trapped ions while preserving the total number of crosslinking points during service.

Notably, our analysis reveals that dynamic networks preserve pore geometries similar to their static counterparts while achieving a significant increase in diffusion coefficients. This enhancement arises from the continuous bond exchange within CANs, which enables a unique "switch-gate" mechanism. By preventing structural limitations such as dead ends, this mechanism facilitates efficient ion transport via enhanced inter-chain hopping.

Moreover, we introduced a method to control the kinetics of the exchange reaction and examined its impact on ion diffusion. We showed that there is an exponential behavior between the overall number of dynamic exchange reactions, $F_{exchange}$, and the Li-ion diffusion coefficient, introducing an important design strategy for regulating ion transport in CANs.

Taken together, our findings demonstrate that ion conductivity in CANs is governed by both network morphology and the dynamic bonds' ability to actively transport ions. More importantly, conductivity can be tuned without altering key geometrical parameters, offering a promising approach for designing ion-conductive materials with preserved mechanical properties.

Conflicts of interest

The authors declare no conflicts of interest.

Data availability

The data supporting this article have been included as part of the SI.

Atomistic simulation details, coarse-grain mapping, polymerization modelling details, residence time calculation, mean-squared displacement (MSD) analysis, exchange bond reaction kinetics, diffusion coefficient and conductivity calculations for TFSI. See DOI: **https://doi.org/10.1039/d5mh00433k**

4. Conclusions

In this study, we observed that tuning network density allows control over the topology and pore size in static polymeric

References

1 Z. Xue, D. He and X. Xie, Poly (Ethylene Oxide)-Based Electrolytes for Lithium-Ion Batteries, *J. Mater. Chem. A*, 2015, **3**(38), 19218–19253.

2 Z. Li, J. Fu, X. Zhou, S. Gui, L. Wei, H. Yang, H. Li and X. Guo, Ionic Conduction in Polymer-based Solid Electrolytes, *Adv. Sci.*, 2023, **10**(10), 2201718.

3 R. Kato, P. Mirmira, A. Sookezian, G. L. Grocke, S. N. Patel and S. J. Rowan, Ion-Conducting Dynamic Solid Polymer Electrolyte Adhesives, *ACS Macro Lett.*, 2020, **9**(4), 500–506.

4 J. L. Olmedo-Martínez, L. Porcarelli, G. Guzmán-González, I. Calafel, M. Forsyth, D. Mecerreyes and A. J. Müller, Ternary Poly (Ethylene Oxide)/Poly (l, l-Lactide) PEO/PLA Blends as High-Temperature Solid Polymer Electrolytes for Lithium Batteries, *ACS Appl. Polym. Mater.*, 2021, **3**(12), 6326–6337.

5 V. St-Onge, M. Cui, S. Rochon, J.-C. Daigle and J. P. Claverie, Reducing Crystallinity in Solid Polymer Electrolytes for Lithium-Metal Batteries via Statistical Copolymerization, *Commun. Mater.*, 2021, **2**(1), 83.

6 X. Wang, M. Wang, H. Chen, Y. Zhang, B. Niu, L. Tian and D. Long, Dynamically Reversible Cross-Linked Polymer Electrolytes with Highly Ionic Conductivity for Dendrite-Free Lithium Metal Batteries, *Chem. Eng. J.*, 2024, 153830.

7 Y. Fan, O. I. Malyi, H. Wang, X. Cheng, X. Fu, J. Wang, H. Ke, H. Xia, Y. Shen and Z. Bai, Surface-Confined Disordered Hydrogen Bonds Enable Efficient Lithium Transport in All-Solid-State PEO-Based Lithium Battery, *Angew. Chem., Int. Ed.*, 2025, e202421777.

8 C.-D. Fang, Y. Huang, Y.-F. Sun, P.-F. Sun, K. Li, S.-Y. Yao, M.-Y. Zhang, W.-H. Fang and J.-J. Chen, Revealing and Reconstructing the 3D Li-Ion Transportation Network for Superionic Poly (Ethylene) Oxide Conductor, *Nat. Commun.*, 2024, **15**(1), 6781.

9 S. Samanta, S. Kim, T. Saito and A. P. Sokolov, Polymers with Dynamic Bonds: Adaptive Functional Materials for a Sustainable Future, *J. Phys. Chem. B*, 2021, **125**(33), 9389–9401.

10 L. Zhang, L. Chen and S. J. Rowan, Trapping Dynamic Disulfide Bonds in the Hard Segments of Thermoplastic Polyurethane Elastomers, *Macromol. Chem. Phys.*, 2017, **218**(1), 1600320.

11 S. Yan, K. Hu, S. Chen, T. Li, W. Zhang, J. Yin and X. Jiang, Photo-Induced Stress Relaxation in Reconfigurable Disulfide-Crosslinked Supramolecular Films Visualized by Dynamic Wrinkling, *Nat. Commun.*, 2022, **13**(1), 7434.

12 S. Ullah, H. Wang, G. Hang, T. Zhang, L. Li and S. Zheng, Poly (Thiourethane-Co-Ethylene Oxide) Networks Cross-linked with Disulfide Bonds: Reinforcement with POSS and Use for Recyclable Solid Polymer Electrolytes, *Polymer*, 2023, **284**, 126318.

13 F. Pei, L. Wu, Y. Zhang, Y. Liao, Q. Kang, Y. Han, H. Zhang, Y. Shen, H. Xu and Z. Li, Interfacial Self-Healing Polymer Electrolytes for Long-Cycle Solid-State Lithium-Sulfur Batteries, *Nat. Commun.*, 2024, **15**(1), 351.

14 H. Wang, Y. Huang, Z. Shi, X. Zhou and Z. Xue, Disulfide Metathesis-Assisted Lithium-Ion Conduction for PEO-Based Polymer Electrolytes, *ACS Macro Lett.*, 2022, **11**(8), 991–998.

15 B. B. Jing and C. M. Evans, Catalyst-Free Dynamic Networks for Recyclable, Self-Healing Solid Polymer Electrolytes, *J. Am. Chem. Soc.*, 2019, **141**(48), 18932–18937.

16 S. Jang, E. I. Hernandez Alvarez, C. Chen, B. B. Jing, C. Shen, P. V. Braun, A. Schleife, C. M. Schroeder and C. M. Evans, Control of Lithium Salt Partitioning, Coordination, and Solvation in Vitrimer Electrolytes, *Chem. Mater.*, 2023, **35**(19), 8039–8049.

17 P. Chakma, Z. A. Digby, M. P. Shulman, L. R. Kuhn, C. N. Morley, J. L. Sparks and D. Konkolewicz, Anilinium Salts in Polymer Networks for Materials with Mechanical Stability and Mild Thermally Induced Dynamic Properties, *ACS Macro Lett.*, 2019, **8**(2), 95–100.

18 Z. Tang, X. Lyu, A. Xiao, Z. Shen and X. Fan, High-Performance Double-Network Ion Gels with Fast Thermal Healing Capability via Dynamic Covalent Bonds, *Chem. Mater.*, 2018, **30**(21), 7752–7759.

19 A. Maitra and A. Heuer, Cation Transport in Polymer Electrolytes: A Microscopic Approach, *Phys. Rev. Lett.*, 2007, **98**(22), 227802.

20 D. Diddens, A. Heuer and O. Borodin, Understanding the Lithium Transport within a Rouse-Based Model for a PEO/LiTFSI Polymer Electrolyte, *Macromolecules*, 2010, **43**(4), 2028–2036.

21 V. Bocharova and A. P. Sokolov, Perspectives for Polymer Electrolytes: A View from Fundamentals of Ionic Conductivity, *Macromolecules*, 2020, **53**(11), 4141–4157.

22 O. Borodin and G. D. Smith, Mechanism of Ion Transport in Amorphous Poly (Ethylene Oxide)/LiTFSI from Molecular Dynamics Simulations, *Macromolecules*, 2006, **39**(4), 1620–1629.

23 D. J. Brooks, B. V. Merinov, W. A. Goddard III, B. Kozinsky and J. Mailoa, Atomistic Description of Ionic Diffusion in PEO–LiTFSI: Effect of Temperature, Molecular Weight, and Ionic Concentration, *Macromolecules*, 2018, **51**(21), 8987–8995.

24 M. Fischer, A. Heuer and D. Diddens, Structure and Transport Properties of Poly (Ethylene Oxide)-Based Cross-Linked Polymer Electrolytes–A Molecular Dynamics Simulations Study, *Macromolecules*, 2022, **55**(22), 10229–10242.

25 J. Lu, A. Barnett and V. Molinero, Effect of Polymer Architecture on the Nanophase Segregation, Ionic Conductivity, and Electro-Osmotic Drag of Anion Exchange Membranes. The, *J. Phys. Chem. C*, 2019, **123**(14), 8717–8726.

26 J. Krajniak, S. Pandiyan, E. Nies and G. Samaey, Generic Adaptive Resolution Method for Reverse Mapping of Polymers from Coarse-Grained to Atomistic Descriptions, *J. Chem. Theory Comput.*, 2016, **12**(11), 5549–5562.

27 S. M. Mousavifard, H. Ghermezcheshme, A. Mirzaalipour, M. Mohseni and H. Makki, PolySMart: A General Coarse-Grained Molecular Dynamics Polymerization Scheme, *Mater. Horiz.*, 2023, **10**(6), 2281–2296.

28 E. Lindahl, B. Hess and D. Van Der Spoel, GROMACS 3.0: A Package for Molecular Simulation and Trajectory Analysis, *Mol. Model. Annu.*, 2001, **7**(8), 306–317.

29 W. F. Van Gunsteren and H. J. C. Berendsen, A Leap-Frog Algorithm for Stochastic Dynamics, *Mol. Simul.*, 1988, **1**(3), 173–185.

30 G. Bussi, D. Donadio and M. Parrinello, Canonical Sampling through Velocity Rescaling, *J. Chem. Phys.*, 2007, **126**(1), 14101.

31 M. Parrinello and A. Rahman, Polymorphic Transitions in Single Crystals: A New Molecular Dynamics Method, *J. Appl. Phys.*, 1981, **52**(12), 7182–7190.

32 T. Darden, D. York and L. Pedersen, Particle Mesh Ewald: An N Log (N) Method for Ewald Sums in Large Systems, *J. Chem. Phys.*, 1993, **98**(12), 10089–10092.

33 W. Humphrey, A. Dalke and K. Schulten, VMD: Visual Molecular Dynamics, *J. Mol. Graphics*, 1996, **14**(1), 33–38.

34 M. Rezayani, F. Sharif and H. Makki, Role of Side-Chain Lengths on Hydronium Mobility in Sulfonated Poly (Ether Sulfone) Proton-Conducting Model Membranes, *J. Phys. Chem. C*, 2023, **127**(18), 8462–8472.

35 L. Wu, X. Zhou, G. Zhang, N. Zhang, Y. Huang, S. Dai and Y. Shen, Tunable OH–Transport and Alkaline Stability by Imidazolium-Based Groups of Poly (2, 6-Dimethyl-1, 4-Phenylene Oxide) Anion Exchange Membranes: A Molecular Dynamics Simulation, *Ind. Eng. Chem. Res.*, 2021, **60**(6), 2481–2491.

36 L. Sarkisov, R. Bueno-Perez, M. Sutharson and D. Fairen-Jimenez, Materials Informatics with PoreBlazer v4. 0 and the CSD MOF Database, *Chem. Mater.*, 2020, **32**(23), 9849–9867.

37 M. Rezayani, F. Sharif, R. R. Netz and H. Makki, Insight into the Relationship between Molecular Morphology and Water/Ion Diffusion in Cation Exchange Membranes: Case of Partially Sulfonated Polyether Sulfone, *J. Membr. Sci.*, 2022, **654**, 120561.

38 M. Rezayani, F. Sharif and H. Makki, Understanding Ion Diffusion in Anion Exchange Membranes; Effects of Morphology and Mobility of Pendant Cationic Groups, *J. Mater. Chem. A*, 2022, **10**, 18295–18307.

39 A. France-Lanord and J. C. Grossman, Correlations from Ion Pairing and the Nernst-Einstein Equation, *Phys. Rev. Lett.*, 2019, **122**(13), 136001.

40 T. A. Wassenaar, K. Pluhackova, R. A. Bockmann, S. J. Marrink and D. P. Tieleman, Going Backward: A Flexible Geometric Approach to Reverse Transformation from Coarse Grained to Atomistic Models, *J. Chem. Theory Comput.*, 2014, **10**(2), 676–690.

41 Q. Zhang, K. Liu, F. Ding and X. Liu, Recent Advances in Solid Polymer Electrolytes for Lithium Batteries, *Nano Res.*, 2017, **10**, 4139–4174.

42 N. S. Grundish, J. B. Goodenough and H. Khani, Designing Composite Polymer Electrolytes for All-Solid-State Lithium Batteries, *Curr. Opi. Electrochem.*, 2021, **30**, 100828.

43 G. Mao, M.-L. Saboungi, D. L. Price, M. B. Armand and W. S. Howells, Structure of Liquid PEO-LiTFSI Electrolyte, *Phys. Rev. Lett.*, 2000, **84**(24), 5536.

44 M. Kunze, E. Paillard, S. Jeong, G. B. Appetecchi, M. Schönhoff, M. Winter and S. Passerini, Inhibition of Self-Aggregation in Ionic Liquid Electrolytes for High-Energy Electrochemical Devices, *J. Phys. Chem. C*, 2011, **115**(39), 19431–19436.

45 K. Timachova, H. Watanabe and N. P. Balsara, Effect of Molecular Weight and Salt Concentration on Ion Transport and the Transference Number in Polymer Electrolytes, *Macromolecules*, 2015, **48**(21), 7882–7888.

46 B. M. Savoie, M. A. Webb and T. F. Miller III, Enhancing Cation Diffusion and Suppressing Anion Diffusion via Lewis-Acidic Polymer Electrolytes, *J. Phys. Chem. Lett.*, 2017, **8**(3), 641–646.

47 A. R. Denton, Effective Interactions in Soft Materials, *Nanostructured soft matter: Experiment, theory, simulation and perspectives*, 2007, pp. 395–433.

48 R. Benassi and F. Taddei, A Theoretical Ab Initio Approach to the S–S Bond Breaking Process in Hydrogen Disulfide and in Its Radical Anion, *J. Phys. Chem. A*, 1998, **102**(30), 6173–6180.

49 K. Yamawake and M. Hayashi, The Role of Tertiary Amines as Internal Catalysts for Disulfide Exchange in Covalent Adaptable Networks, *Polym. Chem.*, 2023, **14**(6), 680–686.

50 B. Li, Z. Zhang, R. Tio, J. Li and T.-P. Loh, An Innovative Strategy for Radical-Mediated, Bidirectional Controlled Disulfide Exchange, *Proc. Natl. Acad. Sci. U. S. A.*, 2024, **121**(50), e2405337121.

51 L. Lin, H. Zou, W. Li, L.-Y. Xu, E.-M. Li and G. Dong, Redox Potentials of Disulfide Bonds in LOXL2 Studied by Nonequilibrium Alchemical Simulation, *Front. Chem.*, 2021, **9**, 797036.

52 Y. Patehebieke, An Overview on Disulfide-Catalyzed and Cocatalyzed Photoreactions, *Beilstein J. Org. Chem.*, 2020, **16**(1), 1418–1435.

53 D. J. Fortman, J. P. Brutman, G. X. De Hoe, R. L. Snyder, W. R. Dichtel and M. A. Hillmyer, Approaches to Sustainable and Continually Recyclable Cross-Linked Polymers, *ACS Sustainable Chem. Eng.*, 2018, **6**(9), 11145–11159.

54 A. M. Stephan, Review on Gel Polymer Electrolytes for Lithium Batteries, *Eur. Polym. J.*, 2006, **42**(1), 21–42.